Pharm Res (2014) 31:335–346
DOI 10.1007/s11095-013-1163-8

RESEARCH PAPER

Compartmental Models for Apical Efflux by P-glycoprotein: Part 2—A Theoretical Study on Transporter Kinetic Parameters

Ken Korzekwa • Swati Nagar

Received: 23 April 2013 / Accepted: 28 July 2013 / Published online: 20 August 2013

ABSTRACT

Purpose The impact of efflux transporters in intracellular concentrations of a drug can be predicted with modeling techniques. In Part 1, several compartmental models were developed and evaluated. The goal of Part 2 was to apply these models to the characterization and interpretation of saturation kinetic data.

Methods The compartmental models from Part 1were used to evaluate a previously published dataset from cell lines expressing varying levels of P-glycoprotein. Kinetic parameters for the transporter were estimated and compared across models.

Results Fits and errors for all compartmental models were identical. All compartmental models predicted more consistent parameters than the Michaelis-Menten model. The 5-compartment model with efflux out of the membrane predicted differential impact of P-gp upon apical *versus* basolateral drug exposure. Finally, the saturable kinetics of active efflux along with a permeability barrier was modeled to delineate a relationship between intracellular concentration with or without active efflux *versus* donor concentration. This relationship was not a rectangular hyperbola, but instead was shown to be a quadratic function.

Conclusions One approach to estimate an *in vivo* transporter effect is to first model an intracellular Km value from *in vitro* data, and use this value along with the appropriate tissue transporter expression levels and relative surface area to calculate the relevant apparent Km (or Ki) values. Together with the results from Part 1, these studies suggest that compartmental models can provide a path forward to better utilize *in vitro* transporter data for *in vivo* predictions such as physiologically based pharmacokinetic modeling.

KEY WORDS compartmental models · intracellular concentrations · kinetics · P-glycoprotein · transporters

K. Korzekwa • S. Nagar (✉)
Department of Pharmaceutical Sciences
Temple University School of Pharmacy
3307 N Broad Street, Philadelphia, Pennsylvania 19140, USA
e-mail: swati.nagar@temple.edu

ABBREVIATIONS

3C	Three-compartment model
5Ccell	Five-compartment model with apical efflux modeled out of the cell
5Cmem	Five-compartment model with apical efflux modeled out of the apical membrane
C_A	Concentration of drug in the apical compartment
C_{AM}	Concentration of drug in the apical membrane compartment
C_B	Concentration of drug in the basolateral compartment
C_{BM}	Concentration of drug in the basolateral membrane compartment
Ccell	Concentration of drug in the cellular compartment
$Ccell_{,AB}$	Concentration of drug in the cellular compartment upon apical drug exposure
$Ccell_{,BA}$	Concentration of drug in the cellular compartment upon basolateral drug exposure
$Ccell_{,pass}$	Concentration of drug in the cellular compartment in the absence of apical efflux
C_{donor}	Concentration of drug in the donor compartment
CLae	Active apical efflux clearance
CLd	Passive diffusional clearance
CLi	Passive diffusional clearance into a membrane compartment
CLo	Passive diffusional clearance out of a membrane compartment
$C_{receiver}$	Concentration of drug in the receiver compartment
CV	Coefficient of variation
IC_{50}	Inhibitor concentration required to cause 50% inhibition
Ki	Inhibition constant for competitive inhibition
Km	Michaelis-Menten constant
Km,app	Apparent Km
Km,app,AB	Apparent Km calculated upon apical drug exposure

Km,app,BA	Apparent Km calculated upon basolateral drug exposure
Kp	Membrane partition coefficient for a drug
MDR1	multidrug resistance 1 gene
MM	Michaelis-Menten
Papp	Apparent permeability
P-gp	P-glycoprotein
PS1/S	Permeability-surface area product normalized by surface area
RMSE	root mean square error
Vmax	maximal velocity

INTRODUCTION

There is an increasing interest in the effect of transporters on the disposition of drugs (1,2). Uptake and efflux transporter activity can increase or decrease intracellular concentrations, respectively. These changes in intracellular concentrations can result in significant differences in target activity (for intracellular targets), distribution (e.g. blood–brain barrier permeability), metabolism, and side effect profiles such as cytochrome P450 inhibition or induction. Also, inhibition of these transporters by other drugs can result in additional drug-drug interactions (DDIs). Regulatory agency guidances state that the kinetic parameters for active transport processes should be used to evaluate the need for clinical DDI studies (3,4). In general, accurate intracellular concentrations are required for pharmacokinetic and pharmacodynamic predictions (5). Therefore, accurate transporter kinetic parameters become necessary inputs for physiologically-based pharmacokinetic (PBPK) and pharmacodynamics models.

It has been reported that apparent kinetic parameters, based on extracellular concentrations may vary with cell type (6,7). A number of investigators have used compartmental models to study the kinetics of transporters (8–11) as well as the interactions between transport and metabolism (12–14). Bentz *et al.* were the first to discuss that the observed Km for an efflux transporter can be very different than the actual Km (15). Korjamo *et al.* suggested that a decrease in the intracellular concentration of efflux transporter substrates was responsible for the shift in observed Km values (6). IC_{50} and Km values were shown by Kalvass and Pollack to be overestimated using extracellular concentrations (16). Shirasaka *et al.* have shown a direct correlation between P-glycoprotein (P-gp) expression and Km,app values (7). Using a three compartment model to calculate intracellular concentrations, Tachibana *et al.* provided more consistent Km estimates across cell lines than is calculated from a Michaelis-Menten (MM) approach (8).

In our previous work (17) and in Part 1, we evaluated compartmental models with explicit membrane compartments to predict intracellular concentrations from bidirectional permeability experiments. In the present study, we used the saturation data for three P-gp substrates in various cell lines reported by Tachibana *et al.* (8), and conducted a theoretical analysis of different compartmental models. The models that were evaluated included a 3-compartment model (3C), a 5-compartment model with efflux out of the cytosol (5Ccell), and a 5-compartment model with efflux out of the apical membrane (5Cmem). Using the Tachibana dataset, we fit saturation curves to obtain kinetic parameters for these models. With the estimated kinetic parameters, we simulated basolateral exposure in each case. An approach to the interpretation of *in vitro* transporter kinetic data is detailed in this report.

MATERIALS AND METHODS

The data from Tachibana *et al.* (8) was digitized to provide C_{donor} and Papp values. The Papp values were used to calculate receiver concentrations assuming 90 min incubations and a 1.0 cm^2 surface area. Mathematica 9 (Wolfram Research) was used for all calculations. For the 3C, 5Ccell and 5Cmem, differential equations for the models in Fig. 1 were used to

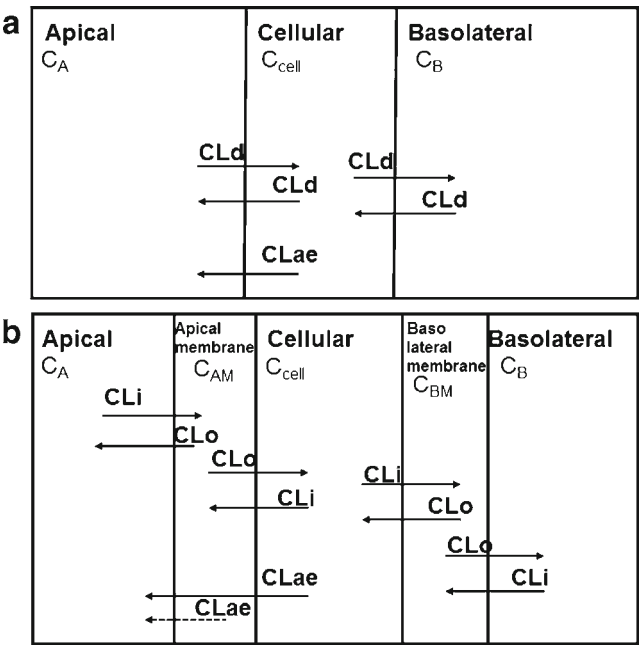

Fig. 1 Compartmental models to predict transporter kinetics. (**a**) A 3-compartment (3C) model was developed with apical, cellular, and basolateral compartments. Diffusional clearance (CLd) with apical efflux clearance (CLae) was modeled. (**b**) A 5-compartment model was developed with apical, apical membrane, cellular, basolateral membrane, and basolateral compartments. Diffusional clearances in (CLi) and out (CLo) of the membranes, with apical efflux clearance (CLae), were modeled. Apical efflux was modeled either out of the cell (5Ccell, *solid arrow*) or out of the apical membrane (5Cmem, *dashed arrow*).

estimate clearance values using the FindFit or NonlinearModelFit routines as described previously (17). For the 3C model, membrane permeability was modeled as a passive diffusion clearance (CLd) which was the same across the apical and basolateral membranes. For the 5C models, the molecule was allowed to partition into the membrane with a CLi term and out of the membrane with a CLo term. The partition constant CLi/CLo was set as the experimental membrane partition coefficient (Kp) for microsomes. Microsomes were used because the endoplasmic reticulum membranes are unsorted membranes and should represent an average of apical, basolateral, and other intracellular membranes. A membrane content of 10% was divided evenly between apical and basolateral membrane compartments (see Part 1 for details).

To fit the Michaelis Menten (MM), 3C, and 5Ccell and 5Cmem models (Fig. 1) to the saturation data, an automated procedure was used. First, a permeability equation that includes MM saturation kinetics for transport and a first order passive diffusion clearance (CLd) for passive permeability, was fit to the experimental data. Equation 1 was used to obtain estimates of CLd, Vmax, and Km,app.

$$Papp\ S = CLd + \frac{Vmax}{K_{m,app} + C_{donor}} \tag{1}$$

where Papp is the apparent permeability, S is the surface area, and CLd is the passive diffusional clearance. This equation represents a permeability-transport saturation curve with a lower plateau composed of passive permeability and transport in the Vmax/Km region, a transition region, and an upper plateau where transport is saturated and passive diffusion dominates. The Km,app is the concentration at the center of the transition region.

Since plateau regions of the saturation curves are well predicted with the MM equation for most compounds and cell lines, parameter estimates with this equation were used in the initial fitting process for the 3C and 5C models. The calculated C_{donor} and $C_{receiver}$ values at 1000 * Km,app in Eq. 1 were used to estimate CLd using the differential equations for the 3C and 5C models as described in detail previously (17). This value and the predicted concentrations at Km,app/1000 were used to estimate CLae. Next, the values of CLd and CLae were used to estimate Km with the experimental saturation curve. Vmax can then be calculated from CLae * Km. The resulting values for CLi, CLae, and Km were then used as initial estimates to simultaneously solve for CLi, CLae, and Km with the experimental saturation curve. This procedure resulted in automated convergence to identical curves and RMSE values for the 3C, 5Cmem, and 5Ccell models. It should be noted that, in contrast to the approach used by Tachibana *et al.*, sink-conditions and steady state are not assumed.

Estimated clearances, Km and Vmax values for each model were used to simulate the saturation profile in the B → A direction. Quinidine simulations were used to display the impact of saturation kinetics on the various intracellular concentrations. The average values of CLi and Km for the different cell lines were used along with the fit values for CLae to generate the concentration profiles for each cell line and for passive diffusion only (when CLae = 0). C_{cell} is determined by both passive diffusion and active transport. In order to evaluate the impact of efflux alone on intracellular concentrations, simulated values for C_{cell} were subtracted from $C_{cell,pass}$ (CLae = 0). This difference ($C_{cell,pass}$-C_{cell}) represents the effect of efflux on C_{cell}.

RESULTS

Kinetic Parameters Estimated with the 3C and 5C Models

Figure 2a–e depict quinidine data for receiver to donor concentration ratio *versus* donor concentrations in 5 cell lines expressing varying levels of P-gp. The MM model was fit to the data (blue curve) to obtain Km,app and Vmax estimates (Table I). Parameter estimates obtained by Tachibana *et al.* with their 3-compartment model are also listed in Table I. The 3C model (Fig. 1a) was fit to the data (Fig. 2a–e, red curve) and yielded similar parameter estimates as Tachibana *et al.*'s model. The Tachibana as well as the 3C models predicted Km estimates across cell lines with lower CVs than the MM model. The 5Ccell and 5Cmem models had RMSEs identical to the 3C model, and all three models yielded overlapping fits (Fig. 2a–e, red curves). Identical fits were also obtained with the 7-compartment model described in Part 1 (data not shown). The 5Ccell model yielded parameter estimates similar to the 3C model. As expected, the 5Cmem model gave different Km estimates compared to all other models (Table I). This is because the apical membrane compartment is the driving compartment for efflux in this model, and this compartment has very different (higher) concentrations as compared with intracellular concentrations. Interestingly, this model resulted in Km estimates with CVs similar to the other compartmental models, and lower CVs than Km,app obtained with the MM model. Figure 2f shows the fold decrease in intracellular concentration as a function of P-gp expression level. As discussed previously (17), the 3C and 5Ccell models show similar decreases in Ccell for the A → B and B → A directions. However, the 5Cmem model predicts a much lower decrease in Ccell in the B → A direction.

Similar to Fig. 2 and Table I, data and model fits for vinblastine and verapamil are depicted in Figs. 3 and 4, and

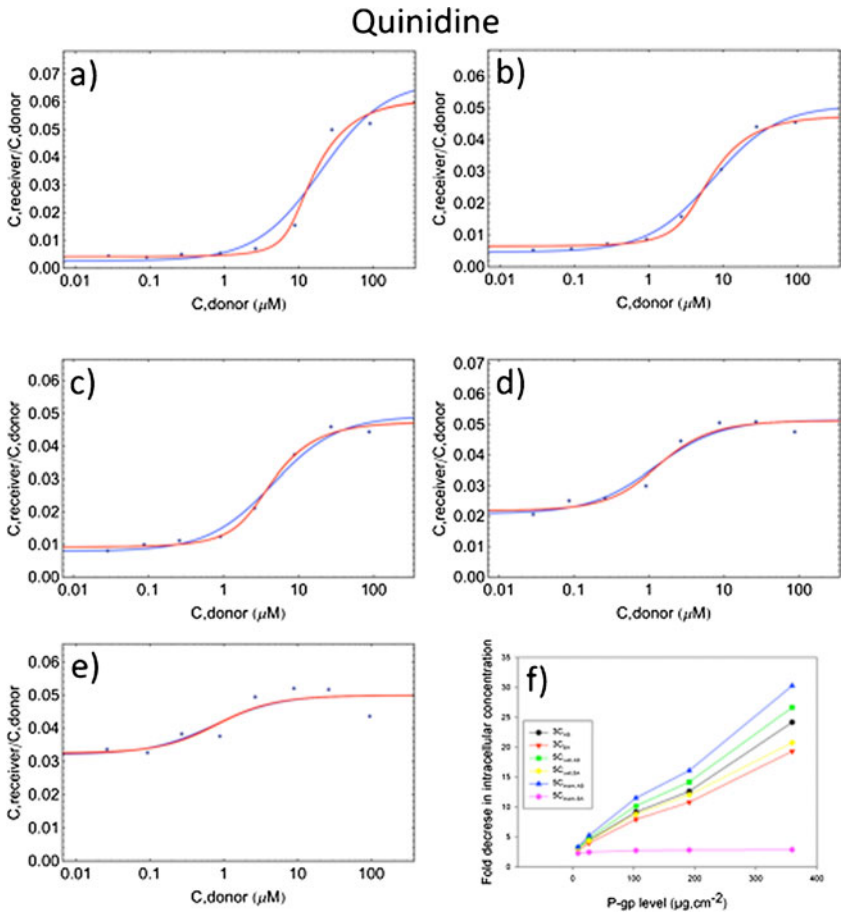

Fig. 2 Quinidine saturation curves and effect of P-gp expression level on intracellular concentration. $C_{receiver}/C_{donor}$ ratio is plotted *versus* C_{donor} from experiments in (**a**) MDR1-MDCKII, (**b**) highly P-gp induced Caco-2, (**c**) P-gp induced Caco-2, (**d**) normal Caco-2, and (**e**) MDR1 knockdown Caco-2 cells. All data are from Tachibana *et al*. (8). *Blue curves* indicate a MM fit, and *red curves* indicate 3C, 5Ccell, and 5Cmem model fits. All three compartmental model fits are overlapping and cannot be distinguished from one another. (**f**) The fold decrease in intracellular concentration relative to donor concentration for each model in the A → B and B → A direction at donor concentration of Km,app/10.

Tables II and III, respectively. The models exhibited the same trend for these 2 substrates as for quinidine i.e. the 3C and 5Ccell models predicted parameters similar to those reported by Tachibana *et al.* The Km estimates across various cell lines were more consistent as compared with the MM model. The 5Cmem model predicted different Km estimates because of a different driving force compartment.

Difference Between Predicted C_{cell} Ratios in the A → B Versus B → A Directions

Next, basolateral exposure was simulated for all three substrates. Listed in Table IV are ratios of predicted intracellular concentrations in the B → A *versus* A → B direction ($C_{cell,BA}/C_{cell,AB}$). The $C_{cell,BA}/C_{cell,AB}$ ratios were generally close to 1 across cell lines and for all 3 substrates with the 3C and 5Ccell models. The 5Cmem model predicted higher $C_{cell,BA}/C_{cell,AB}$ ratios, with the highest ratio for cell lines with the highest P-gp expression – 10.6, 26.8 and 1.9 for quinidine, vinblastine and verapamil respectively.

The concentrations in each compartment for the 5Cmem model were simulated for increasing donor concentrations of quinidine in both the A → B and B → A directions (Fig. 5). Figures 5a–e show compartment concentrations upon apical drug exposure, while Fig. 5f–j exhibit compartment concentrations upon basolateral drug exposure. For apical addition the apical membrane concentration profile (Fig. 5b) is nonlinear between 0 and 10 μM due to the saturation of the transporter. The degree of nonlinearity increases with increasing levels of P-gp expression. This nonlinearity in concentration is propagated to all subsequent compartments (Fig. 5c–e). For basolateral addition (Fig. 5f–j) the impact of the transporter on the compartments prior to the apical membrane (B, BM, and Cell, Fig. 5h–j) is diminished.

Relationship Between Intracellular and Donor Concentrations

For all models, the shape of the saturation curves in Figs. 2, 3, and 4 exhibited a steeper than expected transition (based on MM kinetics alone) between plateaus. In order to explain this shape, a simplified 2-compartmental model depicting a diffusional barrier as well as active efflux out of a transporter model (depicted as a cell compartment for simplicity) was used (Fig. 6a). Saturable transport was modeled with the MM equation. Under the assumptions of initial rate conditions and steady state conditions for C_{cell}, when the rate of change of intracellular concentration is zero, a quadratic relationship

Table I Kinetic Parameter Estimates for Pgp-mediated Transport of Quinidine in Various Cell Lines, Obtained from Different Models

Cell line	P-gp level $\mu g.cm^{-2}$	Km,app μM	Km μM	Vmax/S $\times 10^{-5}$ $\mu M.cm.s^{-1}$	CLd/S[a] $\times 10^{-5}$ $cm.s^{-1}$	Vmax/P-gp $\times 10^{-8}$ s^{-1}	RMSE
MM equation							
MDR1-MDCKII		19.9		36	1.87	0.10	0.005
Highly P-gp induced Caco-2		7.4		9	1.41	0.05	0.001
P-gp induced Caco-2		4.5		5	1.37	0.05	0.002
Normal Caco-2		1.2		1	1.43	0.04	0.002
MDR1 knockdown Caco-2		0.8		0	1.39	0.04	0.003
CV		1.16			0.14	0.44	
Tachibana *et al.*(8)							
MDR1-MDCKII	359.6		0.339	29.09	3.4	0.0809	
Highly P-gp induced Caco-2	191		0.199	6.37	2.5	0.0334	
P-gp induced Caco-2	103.7		0.234	5.13	2.6	0.0495	
Normal Caco-2	26.8		0.23	1.7	2.8	0.0634	
MDR1 knockdown Caco-2	8.71		0.253	0.68	2.7	0.0781	
CV			0.21		0.13	0.33	
3C model							
MDR1-MDCKII			0.255	29.1	3.9	0.081	0.003
Highly P-gp induced Caco-2			0.235	9.2	2.9	0.048	0.001
P-gp induced Caco-2			0.228	5.8	2.9	0.056	0.001
Normal Caco-2			0.190	1.7	3.2	0.065	0.002
MDR1 knockdown Caco-2			0.210	0.748	3.119	0.086	0.003
CV			0.11		0.12	0.24	
5Ccell model (Kp = 875)							
MDR1-MDCKII			0.203	38.0	5.7	0.106	0.003
Highly P-gp induced Caco-2			0.176	12.4	4.6	0.065	0.001
P-gp induced Caco-2			0.175	8.0	4.6	0.077	0.001
Normal Caco-2			0.146	2.3	4.9	0.087	0.002
MDR1 knockdown Caco-2			0.159	0.99	4.8	0.114	0.003
CV			0.12		0.10	0.22	
5Cmem model (Kp = 875)							
MDR1-MDCKII			261	85.8	5.7	0.239	0.003
Highly P-gp induced Caco-2			234	28.8	4.6	0.151	0.001
P-gp induced Caco-2			228	18.5	4.6	0.178	0.001
Normal Caco-2			193	5.4	4.9	0.203	0.002
MDR1 knockdown Caco-2			199	2.2	4.8	0.254	0.003
CV			0.12		0.09	0.21	

ND not determined; *Km,app* apparent Km from the MM fit; *Km* MM constant; *Vmax/S* surface area normalized maximal velocity; *CLd/S* surface area normalized passive clearance; *Vmax/P-gp* P-gp expression level normalized Vmax; *RMSE* root mean square error

[a] CLd is listed for all compartmental model. For the 5C models, CLd is calculated as CLi/2 (24)

between transporter compartment concentration (C_{cell}) and donor concentration (C_A) was derived (Fig. 6b). The impact of efflux transport alone on C_{cell} was evaluated by subtracting C_{cell} from $C_{cell,pass}$ ($C_{cell,pass}$ is calculated at CLae = 0), for the data in Fig. 5c. The fits of the quadratic, MM, and Hill equations to C_{donor} *versus* $C_{cell,pass}$ - C_{cell} are shown in Fig. 7. An Eadie-Hofstee plot of these data (Fig. 7 inset) did not support MM or Hill kinetics, and the quadratic equation provided the best fit to the predicted concentration curve. Thus, the equation derived from the model in Fig. 6 incorporates both passive diffusion and MM efflux, and can be used to describe transporter saturation kinetics in a cell monolayer.

DISCUSSION

Transporter kinetic parameters are necessary when incorporating transport into PBPK models for *in vivo* disposition, and

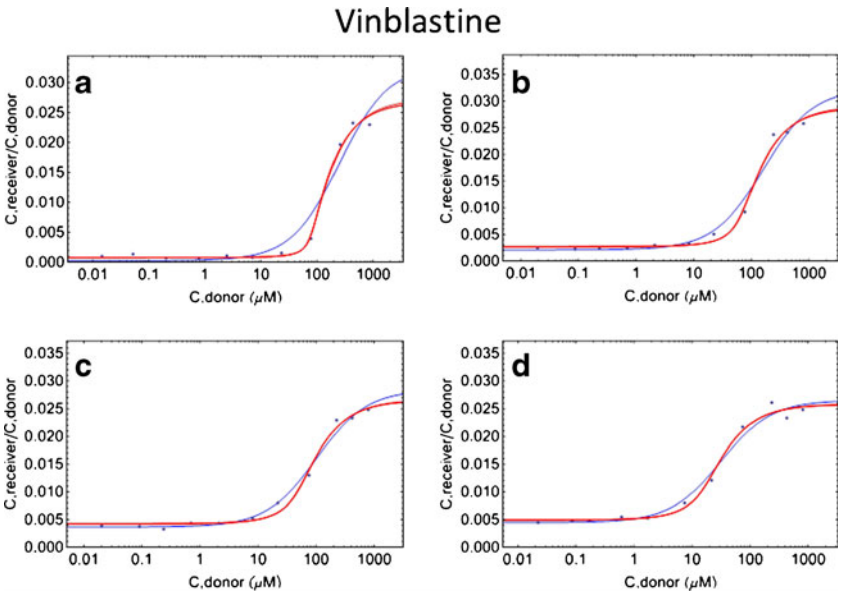

Fig. 3 Vinblastine saturation curves. $C_{receiver}/C_{donor}$ ratio is plotted *versus* C_{donor} from experiments in (**a**) highly P-gp induced Caco-2, (**b**) P-gp induced Caco-2, (**c**) normal Caco-2, and (**d**) MDR1 knockdown Caco-2 cells. All data are from Tachibana *et al*. (8). *Blue curves* indicate a MM fit, and *red curves* indicate 3C, 5Ccell, and 5Cmem model fits. All three compartmental model fits are overlapping and cannot be distinguished from one another.

to predict drug-drug interactions. When estimating efflux transporter kinetic parameters with permeability assays, different cell lines can provide very different Km,app values (7,8). These differences are not random but are due to the effect of the transporter on the concentration of substrate at the transporter active site. Transport activity decreases the concentration resulting in higher Km,app values.

A number of studies have shown that compartmental analyses can provide improved predictions of pharmacokinetic parameters (10,18,19). Tachibana *et al.* have elegantly shown that differences in apparent Km values across cell lines can be explained if calculated intracellular concentrations are used instead of donor concentrations (8). Since P-gp has been suggested to transport substrates directly from the apical membrane (20–23), we have developed models that incorporate explicit membrane compartments (17). These models predict significant differences in intracellular concentrations for apical *versus* basolateral addition (see Part 1), and we have explored the impact of membrane compartments on transporter kinetics. To this end, we have simulated intracellular concentrations for the Tachibana dataset with three models: 3C, 5Ccell, and 5Cmem. In general the 3C and 5Ccell models provide similar parameter estimates and simulated intracellular concentration profiles. The 3C model might be sufficient for efflux out of the cytosol. For the 5Cmem model, the apical membrane concentration drives the active efflux process and marked differences can result.

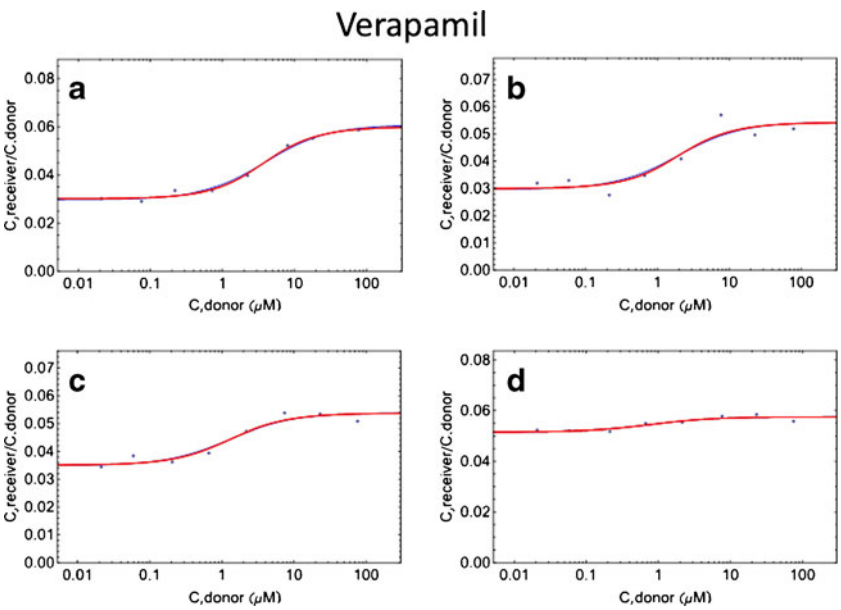

Fig. 4 Verapamil saturation curves. $C_{receiver}/C_{donor}$ ratio is plotted *versus* C_{donor} from experiments in (**a**) MDR1-MDCKII, (**b**) highly P-gp induced Caco-2, (**c**) P-gp induced Caco-2, and (**d**) normal Caco-2 cells. All data are from Tachibana *et al*. (8). *Blue curves* indicate a MM fit, and *red curves* indicate 3C, 5Ccell, and 5Cmem model fits. All three compartmental model fits are overlapping and cannot be distinguished from one another.

Table II Kinetic Parameter Estimates for Pgp-mediated Transport of Vinblastine in Various Cell Lines, Obtained from Different Models

Cell line	P-gp level $\mu g.cm^{-2}$	Km,app μM	Km μM	Vmax/S $\times 10^{-5}$ $\mu M.cm.s^{-1}$	CLd/S[a] $\times 10^{-5}$ $cm.s^{-1}$	Vmax/P-gp $\times 10^{-8}$ s^{-1}	RMSE
MM equation							
MDR1-MDCKII		ND		ND	ND	ND	ND
Highly P-gp induced Caco-2		251		227	0.91	1.19	0.002
P-gp induced Caco-2		163		137	0.90	1.32	0.001
Normal Caco-2		102		70	0.79	2.61	0.001
MDR1 knockdown Caco-2		31		19	0.74	2.21	0.001
CV		0.68			0.10	0.38	
Tachibana *et al.*(8)							
MDR1-MDCKII	360		ND	ND	ND	ND	
Highly P-gp induced Caco-2	191		1.4	113	1.39	0.593	
P-gp induced Caco-2	104		3.0	88	1.44	0.849	
Normal Caco-2	27		3.1	40	1.23	1.493	
MDR1 knockdown Caco-2	9		1.7	18	1.29	2.078	
CV			0.38		0.07	0.53	
3C model							
MDR1-MDCKII			ND	ND	ND	ND	ND
Highly P-gp induced Caco-2			1.07	121	1.6	0.63	0.001
P-gp induced Caco-2			3.04	106	1.7	1.02	0.001
Normal Caco-2			3.97	69	1.6	2.56	0.001
MDR1 knockdown Caco-2			1.61	22	1.5	2.48	0.001
CV			0.55		0.05	0.59	
5Ccell model (Kp = 1550)							
MDR1-MDCKII			ND	ND	ND	ND	ND
Highly P-gp induced Caco-2			0.598	228	3.9	1.19	0.001
P-gp induced Caco-2			1.781	193	4.0	1.86	0.001
Normal Caco-2			2.242	125	3.9	4.67	0.001
MDR1 knockdown Caco-2			0.905	40	3.8	4.58	0.001
CV			0.55		0.03	0.59	
5Cmem model (Kp = 1550)							
MDR1-MDCKII			ND	ND	ND	ND	ND
Highly P-gp induced Caco-2			1445	595	3.9	3.1	0.001
P-gp induced Caco-2			4260	516	4.0	5.0	0.001
Normal Caco-2			5492	348	3.8	13.0	0.001
MDR1 knockdown Caco-2			2209	111	3.8	12.8	0.001
CV			0.55		0.03	0.61	

ND not determined; *Km,app* apparent Km from the MM fit; *Km* MM constant; *Vmax/S* surface area normalized maximal velocity; *CLd/S* surface area normalized passive clearance; *Vmax/P-gp* P-gp expression level normalized Vmax; *RMSE* root mean square error

[a] CLd is listed for all compartmental model. For the 5C models, CLd is calculated as CLi/2 (24)

Comparison of Parameter Estimates for Different Compartmental Models

As seen in Tables I, II, and III, all compartmental models resulted in lower RMSE for the fits compared to the MM model (Eq. 1). Also, the CV for the Km estimates across the cell lines was lower for all compartmental models. The passive permeability values were similar across cell lines for a given compound. Vmax estimates were similar for both the MM, 3C, and 5Ccell models. This can be expected since these values are defined by the plateau regions shown in Figs. 2, 3, and 4. Due to the large partition coefficients, higher estimates for Km and Vmax are obtained when efflux occurs from the membrane (5Cmem).

Kinetic Parameters for Apical Versus Basolateral Exposure

In a previous publication (17) and in Part 1, we have discussed the differential effect of an apical efflux transporter for apical

Table III Kinetic Parameter Estimates for Pgp-mediated Transport of Verapamil in Various Cell Lines, Obtained from Different Models

Cell line	P-gp level $\mu g.cm^{-2}$	Km,app μM	Km μM	Vmax/S $\times 10^{-5}$ $\mu M.cm.s^{-1}$	CLd/S[a] $\times 10^{-5}$ $cm.s^{-1}$	Vmax/P-gp $\times 10^{-8}$ s^{-1}	RMSE
MM equation							
MDR1-MDCKII		3.95		3.4	1.69	0.009	0.001
Highly P-gp induced Caco-2		1.93		1.3	1.51	0.007	0.004
P-gp induced Caco-2		1.28		0.7	1.49	0.006	0.002
Normal Caco-2		0.82		0.1	1.60	0.005	0.001
MDR1 knockdown Caco-2		ND		ND	ND	ND	ND
CV		0.69			0.06	0.27	
Tachibana *et al.*(8)							
MDR1-MDCKII	359.6		0.76	4.53	3.01	0.0126	
Highly P-gp induced Caco-2	191		0.495	2.21	2.75	0.0116	
P-gp induced Caco-2	103.7		0.384	1.1	2.7	0.0106	
Normal Caco-2	26.8		0.37	0.24	2.88	0.0090	
MDR1 knockdown Caco-2	8.71		ND	ND	ND	ND	
CV			0.36		0.05	0.14	
3C model							
MDR1-MDCKII			0.670	5.4	3.8	0.015	0.001
Highly P-gp induced Caco-2			0.388	2.3	3.4	0.012	0.003
P-gp induced Caco-2			0.334	1.3	3.4	0.012	0.002
Normal Caco-2			0.327	0.3	3.7	0.011	0.001
MDR1 knockdown Caco-2			ND	ND	ND	ND	ND
CV			0.38		0.06	0.14	
5Ccell model (Kp = 1430)							
MDR1-MDCKII			0.474	8.0	6.7	0.022	0.001
Highly P-gp induced Caco-2			0.270	3.5	6.2	0.018	0.003
P-gp induced Caco-2			0.233	1.9	6.1	0.019	0.002
Normal Caco-2			0.217	0.4	6.5	0.015	0.001
MDR1 knockdown Caco-2			ND	ND	ND	ND	ND
CV			0.40		0.04	0.15	
5Cmem model (Kp = 1430)							
MDR1-MDCKII			1016	19.6	7.7	0.055	0.001
Highly P-gp induced Caco-2			608	9.0	6.2	0.047	0.003
P-gp induced Caco-2			483	4.6	6.1	0.045	0.002
Normal Caco-2			491	1.1	6.5	0.040	0.001
MDR1 knockdown Caco-2			ND	ND	ND	ND	ND
CV			0.39		0.04	0.13	

ND not determined; *Km,app* apparent Km from the MM fit; *Km* MM constant; *Vmax/S* surface area normalized maximal velocity; *CLd/S* surface area normalized passive clearance; *Vmax/P-gp* P-gp expression level normalized Vmax; *RMSE* root mean square error

[a] CLd is listed for all compartmental model. For the 5C models, CLd is calculated as CLi/2 (24)

versus basolateral addition when efflux occurs from the membrane. Although the experimental dataset used in this study measured permeability in the A → B direction, the kinetic parameters obtained from these analyses can be used to simulate profiles in the B → A direction. This would be relevant in organs such as the liver and the kidney, where the basolateral exposure occurs. As can be seen in Fig. 5 and Table IV, very different profiles in intracellular concentrations are obtained. When efflux transport is modeled from the apical membrane, the nonlinear saturation profile will be most pronounced in the apical membrane compartment. For apical addition, similar decreases in concentrations will be observed in all subsequent compartments. Also, similar nonlinearity will be observed in subsequent compartments, as depicted in Fig. 5b–e. For basolateral addition, the basolateral membrane and intracellular compartments are exposed to drug prior to

Table IV Predicted Intracellular Concentration Ratios in the A → B and B → A Directions from Different models. Intracellular Concentration Ratios were Calculated at Two Concentrations: Km and Km/10

Drug	Cell line	3C model		5Ccell model		5Cmem model	
		CcellBA/CcellAB at Km	CcellBA/CcellAB at Km/10	CcellBA/CcellAB at Km	CcellBA/CcellAB at Km/10	CcellBA/CcellAB at Km	CcellBA/CcellAB at Km/10
Quinidine	MDR1-MDCKII	1.19	1.25	1.17	1.28	1.31	10.58
	Highly P-gp induced Caco-2	1.15	1.17	1.12	1.18	1.37	5.73
	P-gp induced Caco-2	1.14	1.15	1.12	1.16	1.39	4.21
	Normal Caco-2	1.12	1.13	1.09	1.11	1.33	2.13
	MDR1 knockdown Caco-2	1.09	1.09	1.04	1.06	1.17	1.46
Vinblastine	Highly P-gp induced Caco-2	1.07	1.11	1.04	1.16	1.21	26.80
	P-gp induced Caco-2	1.08	1.10	1.06	1.12	1.37	9.18
	Normal Caco-2	1.08	1.09	1.06	1.09	1.45	5.67
	MDR1 knockdown Caco-2	1.07	1.08	1.05	1.08	1.48	4.83
Verapamil	MDR1-MDCKII	1.12	1.14	1.08	1.11	1.27	1.92
	Highly P-gp induced Caco-2	1.11	1.12	1.05	1.08	1.25	1.76
	P-gp induced Caco-2	1.09	1.10	1.03	1.05	1.17	1.49
	Normal Caco-2	1.07	1.07	0.99	1.00	1.03	1.09

the apical membrane. Therefore, the intracellular concentration profile will display a dampened nonlinearity (Fig. 5f–i). Figure 5e and f also show that determining kinetic parameters for apical efflux transporters with apical addition will be more sensitive than basolateral addition.

Model Selection

For all models, the fitted saturation curves in Figs. 2, 3, and 4 are identical, with a steeper than expected (based on MM kinetics alone) transition between plateaus. In general, fitting different models to a data set will normally result in errors that can be used to evaluate these models. In the present study, the 3C, 5Ccell, and 5Cmem models result in indistinguishable predicted saturation curves (Figs. 2, 3, and 4). A familiar analogy is the observation of hyperbolic saturation kinetics for enzymes with very different kinetic schemes. The 3C, 5Ccell and 5Cmem models have been optimized to minimize the error and gave identical model fits and identical errors, albeit with different parameter estimates. Therefore, saturation curves alone cannot be used to evaluate the different compartmental models. Models could be differentiated when considering concentration-time profiles (for example lag times; see Part 1) or differences in binding constants in the A → B and B → A directions.

Nature of the Transporter Saturation Curve

We can examine the increased slopes of the saturation curves in Figs. 2, 3, and 4 (relative to the MM model) using a simplified 2-compartment model shown in Fig. 6. In this model, there is a diffusion barrier between the donor and transporter compartment. For simplicity, we have defined the transporter compartment as the cell, but this could be any compartment from which transport occurs. The resultant relationship between donor concentration and cell concentration with MM saturation of the transporter has been derived under steady-state and initial rate assumptions. This relationship is not rectangular hyperbolic but is quadratic. The impact of the transporter on C_{cell} can be calculated by subtracting C_{cell} from $C_{cell,pass}$. Plotting this difference *versus* C_{donor} results in the saturation curve shown in Fig. 7. The fits of the MM, Hill, and the quadratic equations are also shown. The quadratic equation clearly provides the best fit to the simulated data. Additionally, the Eadie-Hofstee plot of this data (Fig. 7, inset) is not indicative of MM or Hill kinetics.

It should also be noted that the relationships described in Figs. 6, and 7 will be applicable to drug metabolizing enzymes as well. The saturation kinetics of any active process that removes drug from a compartment will be impacted as discussed above, when this compartment is separated from the site of measurement by a diffusional barrier. This has

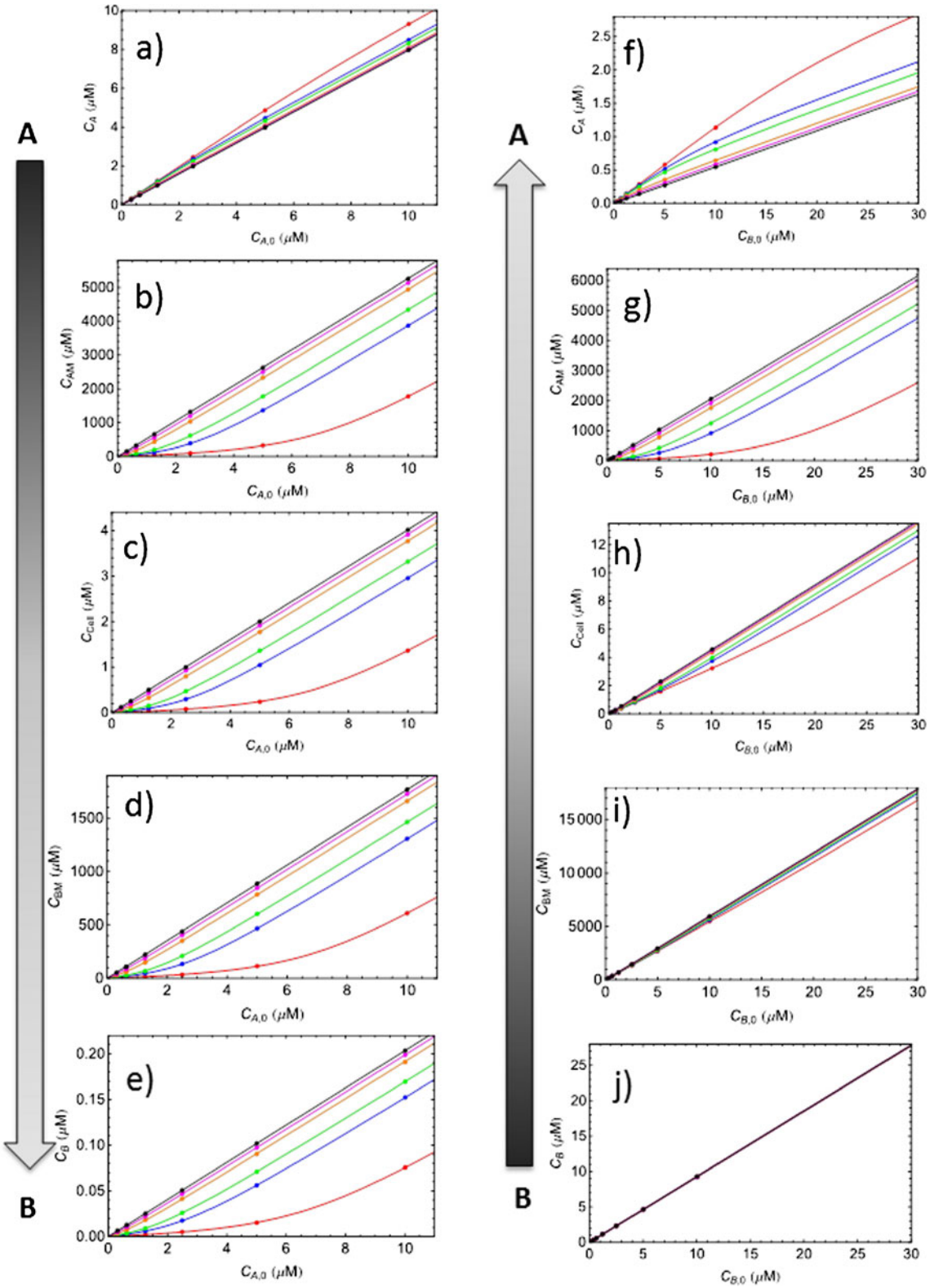

Fig. 5 Predicted A → B and B → A concentration profiles. The 5Cmem model was used to predict concentration profiles for quinidine in each compartment relative to donor concentration, upon apical (**a–e**) or basolateral (**f–j**) drug exposure. Profiles are depicted for apical efflux in MDR1-MDCKII (*red*), highly P-gp induced Caco-2 (*blue*), P-gp induced Caco-2 (*green*), normal Caco-2 (*yellow*), and MDR1 knockdown Caco-2 (*pink*) cells. The profile in *black* is a simulation in the absence of apical efflux. Concentrations shown are apical (**a, f**), apical membrane (**b, g**), intracellular (**c, h**), basolateral membrane (**d, i**), and basolateral (**e, j**).

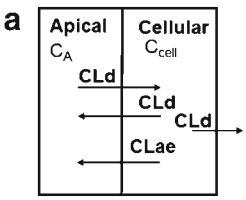

b

1) *Assuming MM saturable transporter kinetics,*

$$CLae = \frac{Vmax}{C_{cell} + Km}$$

The rate of change of Ccell is

$$\frac{dC_{cell}}{dt} = C_A CLd - C_{cell}(2CLd + CLae)$$

At initial rate conditions,

and a steady state assumption for $\frac{dC_{cell}}{dt}$,

$$C_A CLd = C_{cell}\left(2CLd + \frac{Vmax}{C_{cell} + Km}\right)$$

Or,

$$2CLd(C_{cell})^2 + (2CLdKm + Vmax - CLdC_A)C_{cell} - CLdKmC_A = 0$$

The positive solution of this quadratic equation is,

$$C_{cell} = \frac{1}{4CLd}\left(\sqrt{8C_A CLd^2 Km + (-C_A CLd + 2CLdKm + Vmax)^2}\right)$$

2) *When* $CLae = 0, C_{cell} = \frac{C_A}{2}$

Fig. 6 A 2-compartmental model depicting a diffusional barrier as well as active efflux out of a transporter compartment (**a**). For simplicity, the transporter compartment is defined as 'Cell'. Diffusional clearance (CLd) with apical efflux clearance (CLae) was modeled. (**b**) Derivation of a quadratic equation defining the relationship between C_{cell} and C_A in the presence of active efflux as well as a diffusional barrier. The volume of the cell is assumed to be 1.

implications when intracellular transport and elimination processes are considered in relation to plasma concentrations. Either compartmental models or the quadratic relationship in Fig. 6 will correctly describe these relationships.

Since we generally relate pharmacologic activities to unbound plasma concentrations, the most relevant transporter Km (and Ki as well) values are the Km,app for that particular tissue. The Km,app value will be dependent on the characteristics of the tissue including level of P-gp expression and membrane surface area. Since P-gp expression levels in cell models do not necessarily match expression levels in tissues, a Km,app measured *in vitro* may be misleading. As shown in Tables I, II, and III and discussed by Tachibana *et al.* (8), more consistent Km values are calculated with compartmental models than with the MM model. An approach to estimate an *in vivo* transporter effect would be to first model an intracellular Km value from *in vitro* data, and use this value along with the appropriate tissue transporter expression levels and relative surface area to calculate the relevant apparent Km (or Ki) values. For apical exposure (the gut and the brain for P-gp), the 3C and 5C models will give similar results since these models show similar, and sometimes large, fractional decreases in intracellular concentrations due to P-gp. For basolateral exposure (liver and kidney) the 3C and 5Ccell models may over-predict the impact of efflux transport on intracellular concentrations (see Fig. 2f).

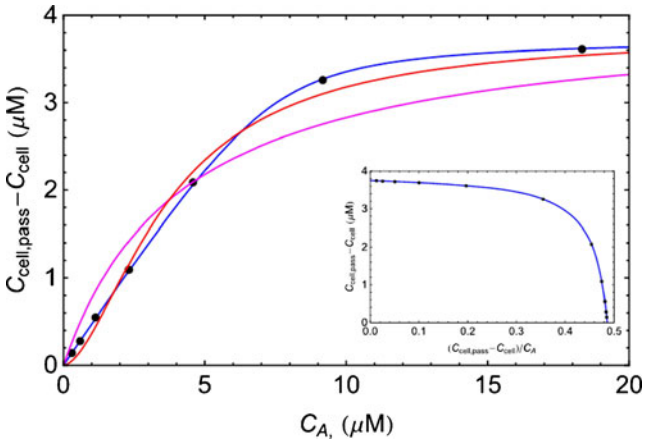

Fig. 7 Impact of efflux transporter on saturation curve of C_{cell}. The simulated difference between Cell in the absence and presence of efflux transport ($C_{cell,pass}$-C_{cell}) is plotted *versus* donor concentration (C_A). MM (*pink*), Hill (*red*), and quadratic (*blue*) equation fits are depicted. Fitting included data from 0 to 300 μM C_A (only 0–20 μM C_A is shown for clarity). The quadratic equation provided the best fit to the simulated data. Inset: Eadie-Hofstee plot of simulated data.

In summary, we have evaluated the use of compartmental models to describe the observed saturation kinetics for P-gp. As discussed by Tachibana *et al.*, efflux transport can decrease intracellular concentrations resulting in different observed saturation curves. All three compartmental models evaluated here adequately describe the impact of efflux transport on permeability across cells with different P-gp levels. The CV for calculated Km values for all three substrates and all three models were lower than the CV for the Km,app values. This suggests that the predicted intracellular concentrations can be used to relate *in vitro* results to *in vivo* effects of efflux transport. Since identical predicted curves were obtained for all compartmental models, this data cannot be used to differentiate between models. This is consistent with results in Part 1, where model errors were generally independent of model complexity. P-gp effluxes substrates directly from the membrane, and explicit membrane models such as the 5Cmem may have some advantages. We have also described the impact of a permeability barrier on saturation kinetics. Taken together, this and previous studies suggest that compartmental models may provide a path forward to utilize *in vitro* transporter data for *in vivo* predictions.

ACKNOWLEDGMENTS AND DISCLOSURES

The authors (KK and SN) acknowledge support from National Institute of General Medical Sciences (grant R01GM104178). The authors would like to acknowledge Drs. Joseph Bentz, Harma Ellens, Cory Kalvass, Caroline Lee, and Sandy Pang for useful discussions.

REFERENCES

1. Giacomini KM, Huang SM, Tweedie DJ, Benet LZ, Brouwer KL, Chu X, *et al.* Membrane transporters in drug development. Nat Rev Drug Discov. 2010;9(3):215–36.
2. Zamek-Gliszczynski MJ, Lee CA, Poirier A, Bentz J, Chu X, Ellens H *et al.* Best practices in determination of transporter kinetic parameters and translational models for human transporter-mediated pharmacokinetics and drug interactions. Clin Pharmacol Ther. 2013; In Press.
3. Drug Interaction Studies — Study Design, Data Analysis, Implications for Dosing, and Labeling Recommendations. FDA Guidance for Industry: http://www.fda.gov/Drugs/GuidanceComplianceRegulatoryInformation/Guidances/default.htm.
4. Guideline on the Investigation of Drug Interactions. EMA Guidline www.ema.europa.eu.
5. Chu X, Korzekwa K, Elsby R, Fenner K, Galetin A, Lai Y *et al.* Intracellular drug concentrations and transporters: measurement, modeling and implications in the liver. Clin Pharmacol Ther. 2013; In Press.
6. Korjamo T, Kemiläinen H, Heikkinen AT, Mönkkönen J. Decrease in intracellular concentration causes the shift in Km value of efflux pump substrates. Drug Metab Dispos. 2007;35(9):1574–9.
7. Shirasaka Y, Masaoka Y, Kataoka M, Sakuma S, Yamashita S. Scaling of in vitro membrane permeability to predict P-glycoprotein-mediated drug absorption in vivo. Drug Metab Dispos. 2008;36(5):916–22.
8. Tachibana T, Kitamura S, Kato M, Mitsui T, Shirasaka Y, Yamashita S, *et al.* Model analysis of the concentration-dependent permeability of P-gp substrates. Pharm Res. 2010;27(3):442–6.
9. Watanabe T, Kusuhara H, Maeda K, Shitara Y, Sugiyama Y. Physiologically based pharmacokinetic modeling to predict transporter-mediated clearance and distribution of pravastatin in humans. J Pharmacol Exp Ther. 2009;328(2):652–62.
10. Ménochet K, Kenworthy KE, Houston JB, Galetin A. Simultaneous assessment of uptake and metabolism in rat hepatocytes: a comprehensive mechanistic model. J Pharmacol Exp Ther. 2012;341(1):2–15.
11. Acharya P, O'Connor MP, Polli JW, Ayrton A, Ellens H, Bentz J. Kinetic identification of membrane transporters that assist P-glycoprotein-mediated transport of digoxin and loperamide through a confluent monolayer of MDCKII-hMDR1 cells. Drug Metab Dispos. 2008;36(2):452–60.
12. Pang KS, Maeng HJ, Fan J. Interplay of transporters and enzymes in drug and metabolite processing. Mol Pharm. 2009;6(6):1734–55.
13. Sun TM, Du JZ, Yan LF, Mao HQ, Wang J. Self-assembled biodegradable micellar nanoparticles of amphiphilic and cationic block copolymer for siRNA delivery. Biomater Engl. 2008;29(32):4348–55.
14. Fan J, Maeng HJ, Pang KS. Interplay of transporters and enzymes in the Caco-2 cell monolayer: I. effect of altered apical secretion. Biopharm Drug Dispos. 2010;31(4):215–27.
15. Bentz J, Tran TT, Polli JW, Ayrton A, Ellens H. The steady-state Michaelis-Menten analysis of P-glycoprotein mediated transport through a confluent cell monolayer cannot predict the correct Michaelis constant Km. Pharm Res. 2005;22(10):1667–77.
16. Kalvass JC, Pollack GM. Kinetic considerations for the quantitative assessment of efflux activity and inhibition: implications for understanding and predicting the effects of efflux inhibition. Pharm Res. 2007;24(2):265–76.
17. Korzekwa KR, Nagar S, Tucker J, Weiskircher EA, Bhoopathy S, Hidalgo IJ. Models to predict unbound intracellular drug concentrations in the presence of transporters. Drug Metab Dispos. 2012;40(5):865–76.
18. Watanabe T, Kusuhara H, Maeda K, Kanamaru H, Saito Y, Hu Z, *et al.* Investigation of the rate-determining process in the hepatic elimination of HMG-CoA reductase inhibitors in rats and humans. Drug Metab Dispos. 2010;38(2):215–22.
19. Fridén M, Bergström F, Wan H, Rehngren M, Ahlin G, Hammarlund-Udenaes M, *et al.* Measurement of unbound drug exposure in brain: modeling of pH partitioning explains diverging results between the brain slice and brain homogenate methods. Drug Metab Dispos. 2011;39(3):353–62.
20. Gottesman MM, Hrycyna CA, Schoenlein PV, Germann UA, Pastan I. Genetic analysis of the multidrug transporter. Annu Rev Genet. 1995;29:607–49.
21. Gottesman MM, Pastan I, Ambudkar SV. P-glycoprotein and multidrug resistance. Current opinion in genetics & development. Elsevier; 1996;6(5):610–617.
22. Hennessy M, Spiers JP. A primer on the mechanics of P-glycoprotein the multidrug transporter. Pharmacol Res. 2007;55(1):1–15.
23. Jin MS, Oldham ML, Zhang Q, Chen J. Crystal structure of the multidrug transporter P-glycoprotein from Caenorhabditis elegans. Nature. 2012;490(7421):566–9.
24. Nagar S, Korzekwa K. Commentary: nonspecific protein binding versus membrane partitioning: it is not just semantics. Drug Metab Dispos. 2012;40(9):1649–52.